Supporting information

Interleaving-Twisted Nanoarchitectured Porous Organic Polymer Synergizes Photoactivity Enhancement and Nanozyme-Powered Microenvironment Remodeling for Advanced Infected Wound Therapy

Zongpeng Zhang,[a, b#] Meiyun Du,[a#] Feng Gao, [#c] Yonglei Qin,[a*] Fei Gao,[a*]Peng Sun[c*]

a. Affiliated Hospital of Shandong Second Medical University, Shandong Second Medical University, Weifang 261053 Shandong, PR China.

b. Weifang Mental Health Center, Weifang 261000 Shandong, PR China.

c. School of Pharmacy, Shandong Second Medical University, Weifang, 261053 Shandong, PR China.

d. Weifang Hospital of Traditional Chinese Medicine, Shandong Second Medical University, Weifang 261041 Shandong, PR China.

# These authors contribute equal to this work.

*Correspondence authors

E-mail: peng1993@sdsmu.edu.cn (P. Sun)

Contents

Section 1. Materials

Section 2. Synthetic Procedures

Section 3. Methods

Section 4. ^{1}H NMR

Section 5. FTIR

Section 6. TGA

Section 7. EDS and elemental content from TEM mapping

Section 8. The UV-vis-NIR absorption spectroscopy of DFP-POP

Section 9. Photothermograms of AMP-POP, ACP-POP, APBP-POP and DFP-POP

Section 10. PCE of different photothermal materials

Section 11. Stability studies of the DFP-POP

Section 12. UV absorption peak changes before and after laser irradiation

Section 13. UV absorption of different concentrations of H_2O_2

Section 14. Synergistic antibacterial graph of DFP-POP at 200 μg/mL

Section 15. Comparison of antimicrobial of different materials at 200 μg/mL

Section 16. Polymers -based antibacterial agent

Section 17. Thermal imaging of mice

Section 18. Healing of different materials after 9 days

Section 19. Supporting References

Section 1. Materials

Materials and General Instruments

1. Materials

LB broth, agar, and bacterial viability kit were purchased from Shanghai Beyotime Biotechnology Co., Ltd. 4-cyanobenzaldehyde was purchased from Anhui Zesheng Technology Co. Propionic acid was purchased from Shanghai Maclaren biochemical technology co., LTD. Hydrochloric acid (HCl), *N,N*-dimethylformamide (DMF), Tetrahydrofuran (THF), dichloromethane (DCM), ethyl acetate (EA) and petroleum ether (PE) were supplied by Sinopharm Chemical Reagent Co., Ltd. The purchased reagents and solvents were used directly without further purification. Ferrocene, dibenzo-18-crown-6 was purchased from Shanghai Haohong Biomedical Technology Co. 1, 3, 5-triphenylbenzene was purchased from Shanghai BiDe Pharmaceutical Technology Co. Tetraphenylmethane was purchased from Anhui Zesheng Technology Co.

2. General Instruments

Liquid ^{1}H NMR spectra (400 MHz) were recorded on a Bruker Avance 400 spectrometer using TMS (for ^{1}H, δ = 0.00) as internal standard. The following abbreviations were used to explain the multiplicities: s = singlet, d = doublet, t = triplet and q = quartet. Caisi Sigma 300 scanning electron microscope (Carl Zeiss Optics (China) Co., Ltd.) was used to obtain scanning electron microscope images. Leica inverted fluorescence microscope (Beijing Shangguang Instrument Co., Ltd.) was used to observe the live/dead staining of bacteria and obtain fluorescence images. HT7700 transmission electron microscope (Hitachi, Japan) was used to photograph bacterial morphology. XRD images were obtained by Smartlab 9kw X-ray diffractometer (Rigaku, Japan) using Scientific Nicolet iS20. Infrared spectra at the wavelength from 4000 to 500 cm^{-1} were recorded using the Fourier transform infrared spectrometer (Thermo Fisher Technology Company) via the potassium bromide pressed-disk technique. The absorbance value was determined by the microplate reader (Burten Instrument Co., Ltd.). The morphologies of powder samples were evaluated by scanning electron Microscopy (SEM, Ultra 55) and transmission electron microscopy

(TEM, Tecnai G2 20 TWIN) via dipping the prepared samples on a Cu-net. Thermo-gravimetric analysis (TGA) were recorded using Microcomputer differential thermal balance (HCT-1, Hengjiu, Beijing, China) analyzer under the protection of N_2. Ultraviolet-visible (UV-vis) spectroscopy of PRSA-Cu were obtained from Shimatsu UV 2600 spectrophotometer (Shimadzu, Japan) from 400 nm to 900 nm. Photothermal/photodynamic experiments employed a semiconductor laser system (MDL-III-638, Changchun New Industries Optoelectronics Technology Co., Ltd.), equipped with beam expanders and homogenizing optical elements to ensure uniform energy distribution of the light spot. The irradiation was performed using a diode laser with a central wavelength of 638 nm, selected to match the absorption peak of the DFP-POP material with a tunable range of 0.5–2.0 W cm^{-2} for dose-dependent studies. The output was calibrated using a standard power meter to ensure accuracy. A standardized exposure time of 10 min was applied for most experiments. Timing was controlled digitally with minimal error (<1%).

Section 2. Synthetic Procedures

2.1 Synthesis of tetra(4-acetylphenyl)methane

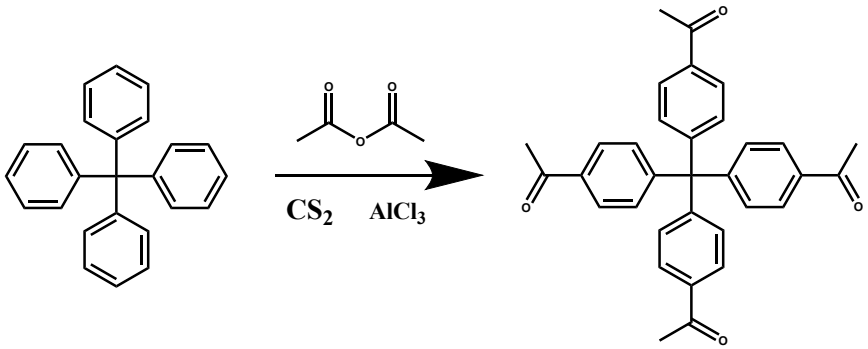

Tetraphenylmethane (0.65 g, 2 mmol), acetyl chloride (0.80 g, 10.2 mmol), aluminium chloride (1.34 g, 10 mmol) and were added to a 250 mL single-necked flask containing carbon disulfide (CS_2, 100 mL). The mixture was heated to 60°C for 18 h. After cooling, the CS_2 was removed by filtration, then the filtrate was added to methylene chloride to dissolve, ice water and concentrated hydrochloric acid were added. The precipitate was extracted when it was completely dissolved. The organic layer was then dried with anhydrous sodium sulfate, filtered to remove the sodium sulfate. And the solvent was removed in vacuum. Chromatographic purification on

silica gel (dichloromethane/hexane) gave tetrakis(4-acetylphenyl)methane (0.40 g) as a colorless powder (yield: 75%). ^{1}H NMR (d6-DMSO, 400 MHz) δ 2.54 (s, 12H), 7.40 (d, 3J = 7.2 Hz, 8H), 7.92 (d, 3J = 8 Hz, 8H).[1]

2.2 Synthesis of 4',4''(5'')-Diacetyldibenzo-18-CROWN-6

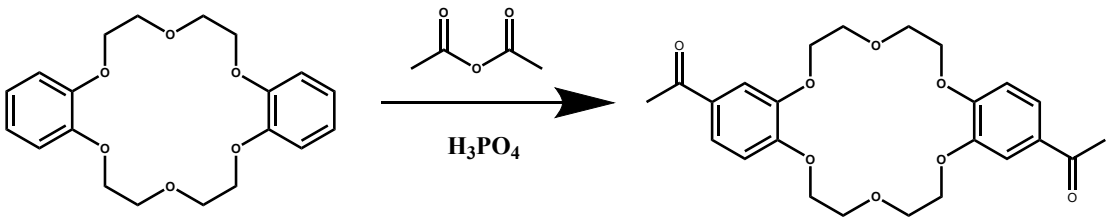

Dibenzo-18crown-6 (1 g, 2.78 mmol) and acetic anhydride (7 ml, 70 mmol) were added to a 100 ml three-necked flask. Then, 3.05 ml of phosphoric acid was added to the reaction system, which was heated to 60^{o}C for 4 h. Afterwards, the reaction system was cooled down to room temperature, following by the injection of cold water was (50 ml) to give a white solid. The solid was obtained by filtration and purified by column chromatography to give white product (Yield 95%). ^{1}H NMR spectrum (300 MHz, $CDCl_3$), δ, ppm (J, Hz): 2.54 (6H), 3.99 (8H, t), 4.20 (8H, t), 6.81 (2H, m), 7.48 (2H, m), 7.53 (2H, m).[2]

2.3 Synthesis of 1,3,5-tris(4-acetylphenyl)benzene

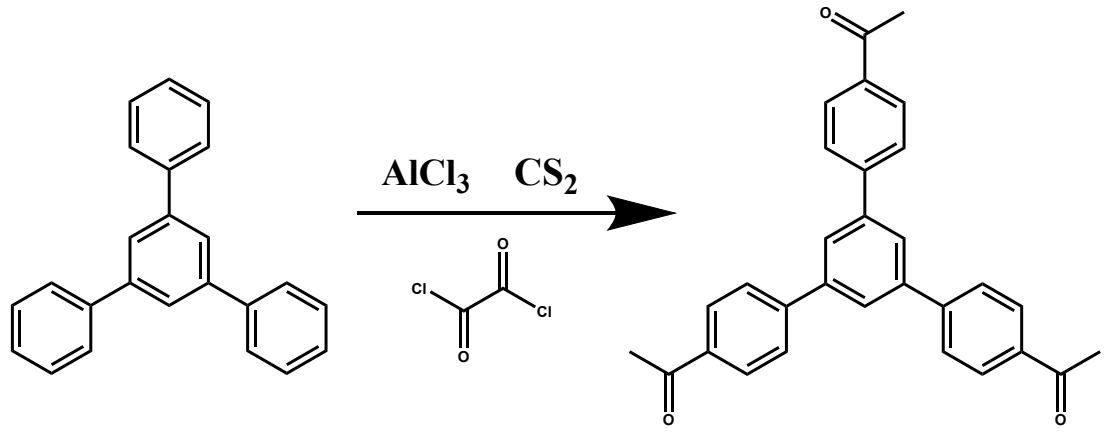

Under the ice bath, $AlCl_3$ (17.0 g, 127 mmol) was dissolved in 75 mL CS_2. Then, acetyl chloride (10.5 g, 9.47 mL) and 1,3,5-triphenylbenzene (10.0 g, 32.6 mmol) pre-dissolved in 100 mL CS_2 was added dropwise. The reaction system was gradually returning to room temperature. Then, the mixture was heated to 50 ^{o}C under reflux for 5 h. Afterwards, the reaction system was cooled to room temperature, which was

continued stirring for 15 h. The reactants were poured into ice water, following by the injection of 50 mL HCl and 200 mL CH_2Cl_2. The organic phase was washed three times with NaCl and sodium hydroxide solution, then dried with anhydrous magnesium sulfate. And the solvent was removed by rotary evaporator. And the crude product was purified by column chromatography to obtain a rice-white solid (yield=86%). ^{1}H NMR (CDCl3, 400 MHz): δ (ppm) 2.65 (s, 9H), 7.78 (t-d, 6H), 7.85 (s, 3H), 8.08 (t-d, 6H).[3]

2.4 Synthesis of 1,1'-diacetylferrocene

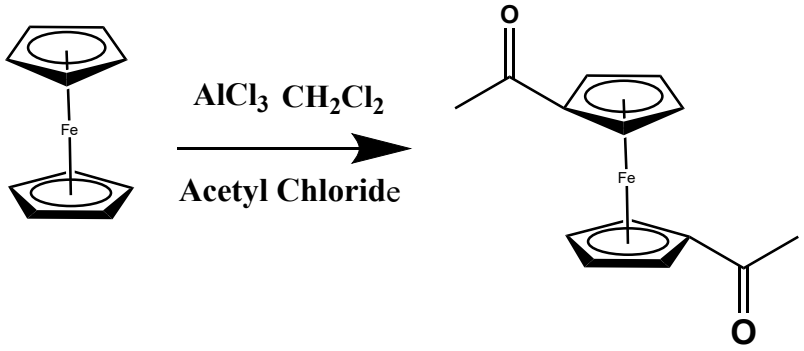

$AlCl_3$ (24 g, 0.17 mol) and dry CH_2Cl_2 60 mL were added to a three-necked flask. Ferrocene (9 g, 0.05 mol), dichloromethane (80 ml) and acetyl chloride (18 ml, 0.24 mol) were added to the three-necked flask drop by drop. Under argon gas protection, the mixture was heated and refluxed for 2 h. It was then cooled down to room temperature, and the reactants were poured into ice water. The crude product was extracted with CH_2Cl_2 for 3 times. And the organic solvent was removed under reduced pressure and recrystallised from ethanol (yield=90%). ^{1}H NMR (270 MHz; d_6-DMSO): 4.74 (4H, t, J 2 Hz), 4.60 (4H, t, J 2 Hz), 2.33 (6H, s). [4]

2.5 Synthesis of 5,10,15,20-tetrachloro(4-cyanophenyl)porphyrin

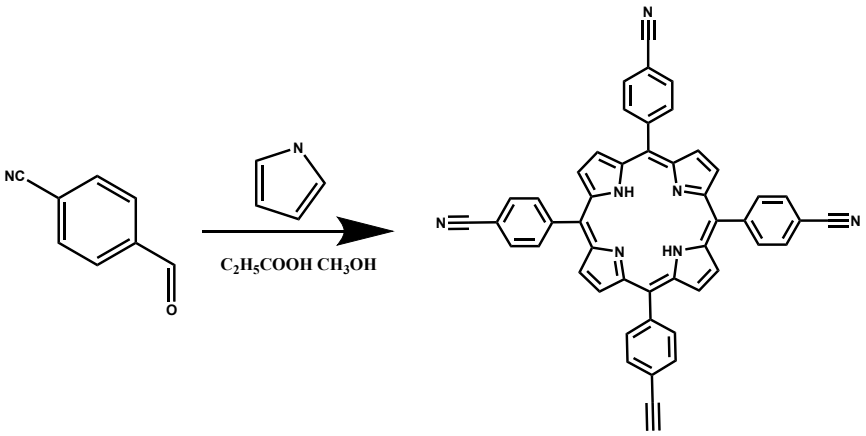

A 250 mL three-necked flask was charged with redistilled pyrrole (7 mL, 100 mmol) and 4-cyanobenzaldehyde (10.0 g, 14 mmol). Then, 400 mL of propionic acid was added into the reaction system. Under argon atmosphere, the reaction system was heated to reflux for 1 h. After, the reaction system was cooled to room temperature naturally, which was filtered and washed with methanol until the filtrate was clarified. The product was then washed with 100 mL of lukewarm water at 50°C and dried under vacuum in an oven at 80°C overnight.

2.6 Synthesis of H_2TDPP

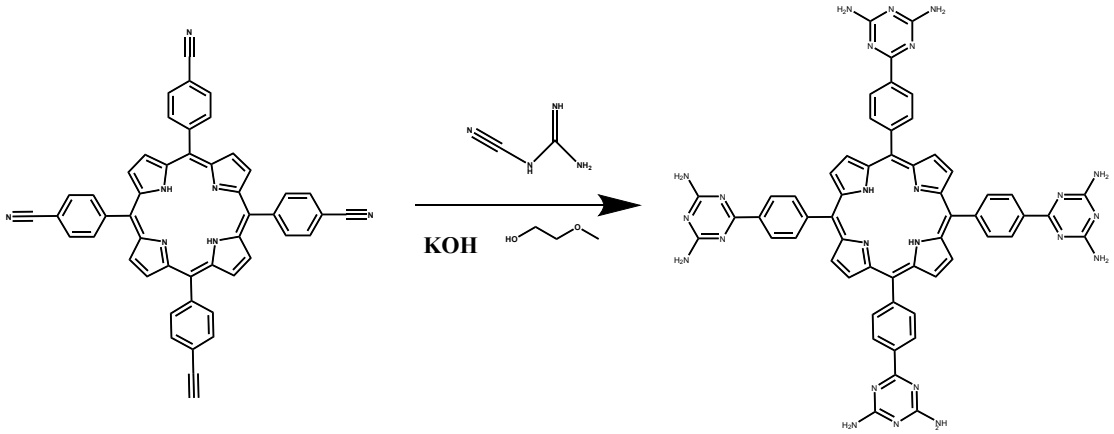

5,10,15,20-tetrachloro(4-cyanophenyl)porphyrin (500 mg, 0.8 mmol) was added to a three-necked flask and a mixture of dicyandiamide (350 mg, 4.1 mmol) and potassium hydroxide (300 mg, 5.3 mmol) pre-dissolved in 2-methoxyethanol (20 mL) was mixed with the above ingredients. Under the argon protection, the reaction system was refluxed for 48 h. The product was then washed with lukewarm water and dried under vacuum in an oven at 70°C overnight to obtain the final product as purple powders. ^{1}H-NMR: (500 MHz DMSO-d6): δ= 8.92 (s, 8H); 8.71 (d, 8H); 8.35 (d, 8H); 6.89 (s, 16H). [5]

2.7 Preparation of POPs

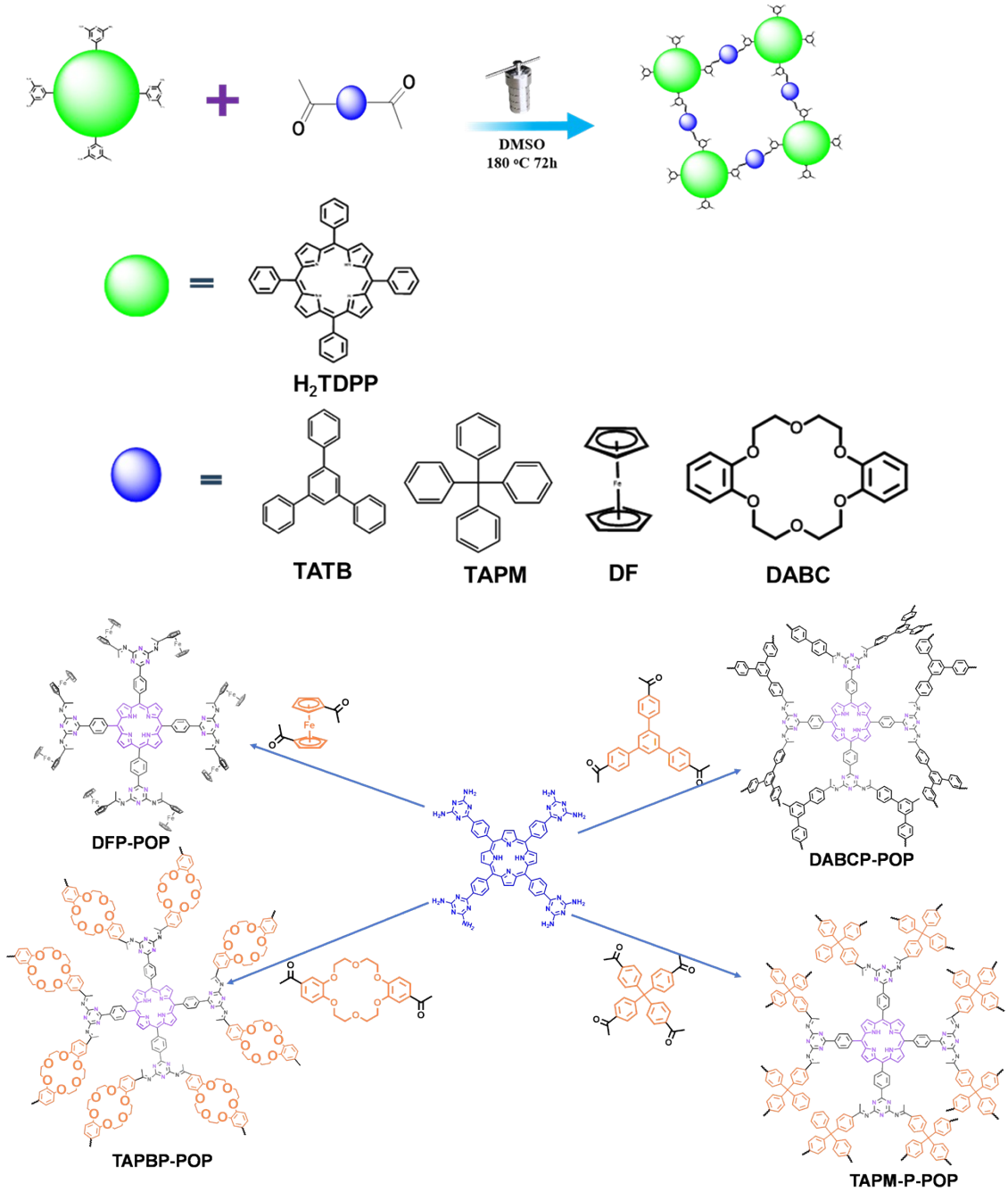

Scheme S1. Typical structure of final POPs

Preparation of DF-POP

To an autoclave was added acetyl monomer (DF) and H_2TDPP (feedstock ratio 4:1), followed by about 25 mL of DMSO and purged with argon for about 3 min. The reaction mixture was heated under nitrogen protection at 180 °C for 72 h. After cooling to room temperature, the reaction was filtered to give a black foamy substance, which was washed successively with CH_3OH, CH_2Cl_2 and THF. The synthesized solid was

dried in a vacuum oven at 120 °C overnight to give a black powder.[6]

Preparation of TAPBP-POP, DABCP-POP, and TAPMP-POP.

A series of control POPs (Scheme S1), including the TAPBP-POP, DABCP-POP, and TAPMP-POP, were synthesized using a similar synthetic approach to ensure structural comparability. Each polymer was prepared by reacting H_2TDPP with the corresponding polyacetylated bridging monomer, 1,3,5-tris(4-acetylphenyl)benzene (TAPB), 4',4'',5''-diacetyldibenzo-18-crown-6 (DABC), or tetra(4-acetylphenyl)methane (TAPM), under identical reaction conditions. The feedstock molar ratio between the acetyl groups (from the bridging monomer) and amino groups (from H_2TDPP) was maintained at 1:1 to ensure full stoichiometric balance and maximize polymerization efficiency. The same workup procedure, including filtration, sequential solvent washing, and vacuum drying, was applied to obtain each polymer in pure form as a dark-colored solid.

Section 3. Methods

In this work, key assays, such as antibacterial tests, hemolysis assay, cytotoxicity test, cell migration assay, blood routine tests and *In Vivo* animal studies were performed in triplicate.

3.1 Stability study of DFP-POP

Stability of DFP-POP in different pH liquids: DFP-POP solution with pH 1.5, 2.5, 3.5, 4.5, 5.5, 6.5 with a concentration of 200 μg/mL was kept for 5 days. The UV absorption values at 638 nm were determined using a UV spectrophotometer.

Photostability of DFP-POP: Water configuration for DFP-POP to 300 μg/mL. After irradiation with a 638 nm infrared laser, five on/off cycles were performed, and the cycle was cooled down and the UV absorption was detected by a UV spectrophotometer.

Stability of DFP-POP in different solvents:

Stability in water: DFP-POP at a concentration of 200 μg/mL were dispersed in different solvents. On day 0, after the laser irradiation, the data were detected and recorded by the infrared thermal imager. It was then placed in the solvent for 15 days, again after laser irradiation with the same laser parameters as on day 0, and data were

recorded via a thermal imager.

Stability in the DMSO: DFP-POP with 200 μg/mL of DMSO configuration was used to determine the degree of UV absorption attenuation of DPBF after DFP-POP laser irradiation on days 1,2, and 4.

3.2 Photothermal performance detection

Water solutions of DFP-POP at different concentrations of 0, 100, 200, 300, 400, 500 μg/mL, were added to the 2 mL ep tube and the total volume of liquid in all ep tubes was 1 mL. The samples were irradiated with 638nm under laser at a power density of 1 W cm^{-2} (10 min). The temperature value will be displayed on the thermal imaging camera, and the temperature that rises within 10 min will be taken every 50 s. Afterwards, we recorded the highest temperature of the different concentrations for 10 min through the thermal imager, and made dot line charts with the concentration. In addition, DFP-POP aqueous suspension (300 μg/mL) was provided with 638 nm laser with power density of 0.5, 1, 1.5, and 2 W cm^{-2} for 10 min, and data were taken every 20 s. Subsequently, the thermal stability of DFP-POP was evaluated by cyclic irradiation experiments with on/off laser irradiation cycles. In short, the configured material suspension is irradiated by the infrared laser with the same laser parameters as above. After 10 min of irradiation, the laser was turned off to cool DFP-POP naturally to room temperature without external force. Afterward, the same cycle was repeated four times to record the temperature changes throughout the cycle. One link of the cycle is drawn separately, and the photothermal conversion efficiency is calculated by the temperature change during the descent process. The calculation formula is as follows:

$$\eta = \frac{hS(T_{max} - T_{surr}) - Q_{Dis}}{I(1 - 10^{-A638})} \times 100\% \quad \textbf{(S1)}$$

Where “h” represents the heat transfer coefficient; “S” represents the surface area of the container; "Tmax" is the equilibrium temperature displayed after 10 min of irradiation; "Tsurr" represents the ambient temperature; "Q_{Dis}" is the heat dissipation of the test unit; "I" represents the laser power density value of the 638 nm laser; and “A_{638}” is the absorbance of DFP-POP aqueous suspension at 638 nm.

$$hS = \frac{m_{H_2O} C_{H_2O}}{\tau_s} \quad \textbf{(S2)}$$

$$\textbf{t= -}\tau_S \textbf{ (Inθ) (S3)}$$

Where "m_{H_2O}"represents the mass of the solvent water, here is 1g; "C_{H_2O}" indicates the stated heat capacity (4.2 J/g). "τ_s" represents a negative log of the cooling time versus the temperature. 'θ' is the ratio of ΔT and Tmax. And "t" is the cooling.

In this work,

Tmax-Tsurr=57.1-27.4=29.7; A638 = 2.306; I=1.0 W cm^{-2};

η (%)=[hS (Tmax – Tsurr) – Qdis] / I ($1-10^{-A638}$) = 43.98%

3.3 Photodynamic performance test

Firstly, a DMSO solution containing both monomer and polymer were prepared, adjusting the concentration to facilitate the measurement of UV absorption. Next, DPBF probe solution was created by mixing 3 mL of DMSO with 50 μL of DPBF, ensuring that the absorbance is approximately 1.0. To establish the probe's stability, the UV absorption was measured after 0, 1, 2, 4, 6, 8, and 10 min of irradiation.

Subsequently, 50 μL of the DPBF probe solution was introduced into the previously prepared solution, maintaining the same irradiation intervals as before. The UV absorption post-irradiation for both H2TDPP and DFP-POP were individually assessed, and plotting the corresponding results. To calculate the percentage reduction, the UV absorption at 421 nm was compared with the material's inherent UV absorption prior to irradiation. To further investigate the stability, DFP-POP was subjected to irradiation for 2, 4, and 6 min, and then DPBF was incorporated to test its capacity to generate singlet oxygen ($^1O_2$) using the aforementioned methodology.

3.4 Hydroxyl radical generation ability test

3,3′,5,5′-tetramethylbenzidine (TMB) is a chromogen, which oxidizes TMB to oxTMB in the presence of ROS. And the solution changes from anhydrous to blue. However, catalase can catalyze the disproportionation of H_2O_2 and produce oxygen. Based on this, first, we configured TMB, H_2O_2 + TMB, and TMB + H_2O_2 + DFP-POP, where the TMB and H_2O_2 concentration is 75 μL/mL, and the DFP-POP concentration

is 400 μg/mL. The total volume of was 1 mL to detect their UV absorption. To further demonstrate that DFP-POP can produce correlated effects, the material was made with an EPR to detect its signal generation. Thereafter, a total volume of 1 mL of 100, 200, 300, 400 and 500 μg/ml at pH 5.5 was configured to detect UV absorption at different concentrations under the same pH conditions. The concentration was set to 400 μg/ml and mated to 1 ml with PBS of pH=1.5, 2.5, 3.5, 4.5, 5.5, and 6.5, and their UV absorption was detected under a UV spectrophotometer.

3.5 CAT-like enzyme activity test

According to previous reports, there may also be CAT-like enzyme activity that catalyzes the production of oxygen and water from H_2O_2. To verify this conjecture, first we measured the UV absorption of different concentrations of H_2O_2 (100 mM, 50 mM, 25 mM, 12.5 mM and 6.25 mM). The DFP-POP concentration was configured to be 200 μg/mL and the H_2O_2 concentration to be 25 mM. The assay was carried out every 10 min starting from 0 min and the decreasing trend of the curve was observed and compared with the blank (no DFP-POP added) group.

3.6 Testing of the antimicrobial properties in vitro

According to the previous experiments, in order to achieve a better comparison, *S. aureus* and *E. coli* were used as representatives of Gram-positive and Gram-negative bacteria, which were utilized to test the antimicrobial properties of DFP-POP. Both bacteria were treated by eight groups, including control group, DFP-POP group, H_2O_2 group, DFP-POP + H_2O_2 group and the laser irradiation group corresponding to these four subgroups more. In the above groupings. The total volume of liquid in each group was 1 mL, the concentration of bacterial fluid was 100 μL/mL, the concentration of DFP-POP was 200 μg/mL, and the concentration of H_2O_2 was 10 μL/mL. All of the groups were in neutral PBS, except for the DFP-POP + H_2O_2 and its laser group, which were in PBS with pH=5.5. Compared to the group with no laser, the laser group was required to irradiate the cells with a 638 nm. The laser group needed to be irradiated with 638 nm infrared laser at a power density of 1W cm^{-2} for 10 min. Finally, the mixed bacterial solution was incubated in a shaker at 37°C for 24h, and 100 μL of the bacterial solution was transferred to the solid medium to observe the morphology and to count

the number of colonies. And the antimicrobial effect was evaluated by comparing with control group.

3.7 Bacterial live/dead staining

Bacteria were stained by SYTO-9 and PI to differentiate between live and dead bacteria under a fluorescence microscope. SYTO-9 penetrates the cell membranes of all bacteria and labels them green, while PI only penetrates the cell membranes of damaged bacteria, labels them red, and neutralizes the green color of SYTO-9 to give a yellow color. Bacterial grouping was the same as in vitro antibacterial grouping. From each group of ep tubes, 400 μL of solution was removed with 100 μL of *S. aureus* or *E. coli* (1×10^8 CFU/mL), 20 μL of SYTO-9 (1.0×10^{-3} M) and 20 μL of PI (1.5×10^{-3}M) were added, and the solution was incubated for 15 min in darkness at 37°C. After, the bacteria were removed by centrifugation to remove the excess SYTO-9 and PI, and then the bacteria were resuspended with 50 μL PBS. The images were observed by inverted fluorescence microscopy.

3.8 The state of the bacteria under TEM

The above treated solution was added to 2.5% glutaraldehyde solution and fixed at 4 °C for 24 h, after which it was washed three times with PBS, embedded and closed with agar. The bacteria were treated with 30%, 50%, 70%, 90%, 95% and 100% concentration of ethanol solution in sequence for 10 min to dehydrate them, after which, they were treated with acetone for 3h and embedded by gradient osmosis. Finally, the bacteria were negatively stained, fixed on a nickel grid and observed by transmission electron microscopy.

3.9 Hemolysis assay

Blood was obtained from Balb/c mice, and the obtained fresh blood was centrifuged (10000 rpm, 10 min), the supernatant was removed, and erythrocytes were collected. Subsequently, PBS was added for washing at a volume ratio of approximately 1:1 to erythrocytes, centrifuged to remove the supernatant, and repeated four times. Then the erythrocytes were mixed with PBS buffer 3:11, and the mixed erythrocytes were mixed with DFP-POP (concentrations of 50, 100, 150, 200, 300, and 400 μg/mL) at a ratio of 1:9 (v/v), and incubated at 37°C for 4 h. 100 μL of the supernatant of each tube was

added into a 96-well plate, and absorbance was measured by an enzyme marker. Distilled water was used as positive control and PBS group was used as negative control. The calculation formula is as follows:

$$Hemolysis\ (\%) = \frac{A - A_n}{A_p - A_n} \times 100\% \quad \textbf{(S4)}$$

A: Absorbance obtained from the supernatant after addition of DFP-POP to the erythrocytes.

An: absorbance of erythrocytes mixed with PBS (negative control).

Ap: absorbance of erythrocytes mixed with distilled water (positive control).

3.10 MTT experiment

In 96-well plates, L929 cells were inoculated at a density of 5×10^3 per well with 100 μL of cells per well, and the plates were liquid-sealed around the edges with 100 μL PBS to prevent excessive evaporation. After incubation for 24 h, different concentrations of DFP-POP (concentrations of 100, 200, 300, 400, 500 μg/mL) were added, the supernatant was discarded after standing for 24 h, 10 μL MTT (5 mg/mL) was added to each well, after 4h, the supernatant was aspirated, 100 μL of DMSO was added, and the absorbance was measured by an enzyme marker after standing for about 10 min. Each set of experiments was repeated 3 times.

3.11 Cell scratches test

The migration ability of cells was tested by cell scratch assay. Cells were inoculated into 6-well plates with approximately 5×10^3 cells per well and cultured for 24 h. Cellular excretions were washed off with PBS, cells were scratched with a sterile lance tip, different concentrations of DFP-POP were added, followed by rinsing of the cells with PBS, and phase-contrast images were taken using a microscope at 0 and 24 h and 48 h, respectively The distance travelled by the cells was measured using Image J software and the percentage of wound healing was calculated.

3.12 Wound healing experiment on the back of mice

Female Balb/c mice of 5 weeks of age and weighing around 17 g were used to establish wound trauma model. The mice were randomly divided into 9 groups, namely: Blank, Control, H_2O_2, H_2O_2 + laser, DFP-POP, Laser, DFP-POP + laser, DFP-POP + H_2O_2,

DFP-POP + H_2O_2 + laser group, and 6 mice in each group. Prior to formal infection, each group of mice will be weighed and treated with anaesthesia except for the blank group, the hair on the back will be shaved off and disinfected with 75% ethanol to form a wound with a radius of about 5 mm, where S. aureus (1×10^6 CFU/ML) will be added to the wound, and the different subgroups will be treated after 24 h of infection. In the above treatment groups, DFP-POP was added at a concentration of 200 μg/mL. H_2O_2 was added at a concentration of 10 μL/mL. The laser irradiation power was 1.0 W cm^{-2} and the irradiation time was 10 min. Changes in the back wounds of the mice were recorded on days 1, 3, 6, and 9, and the body weights of the mice were monitored daily, and the changes in body weight and the area of the back wounds were plotted. The mice were anaesthetised on day 9 and the eyeballs were removed to obtain blood, after which the mice were executed and their back wounds and major organ tissues (heart, liver, spleen, lungs, kidneys) were fixed in 10% formalin. Then H&E staining and Masson trichrome staining were performed. Blood was obtained 2 mL per tube for routine blood tests.

3.13 Statistical Analysis

Data are expressed as mean ± SD. All statistical analyses were performed using SPSS 16.0 software. Differences between groups were analyzed by Student's t-test, and a P-value < 0.05 was considered statistically significant.

Section 4. 1H NMR

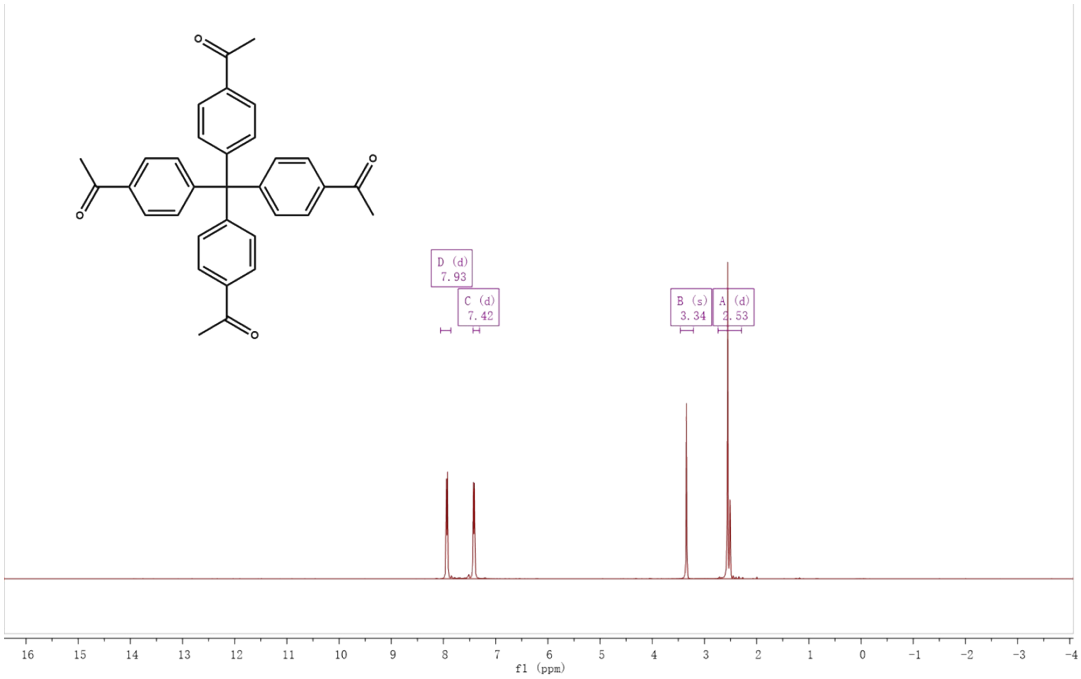

Figure S1. [1]H NMR of tetra(4-acetylphenyl)methane (TAPM)

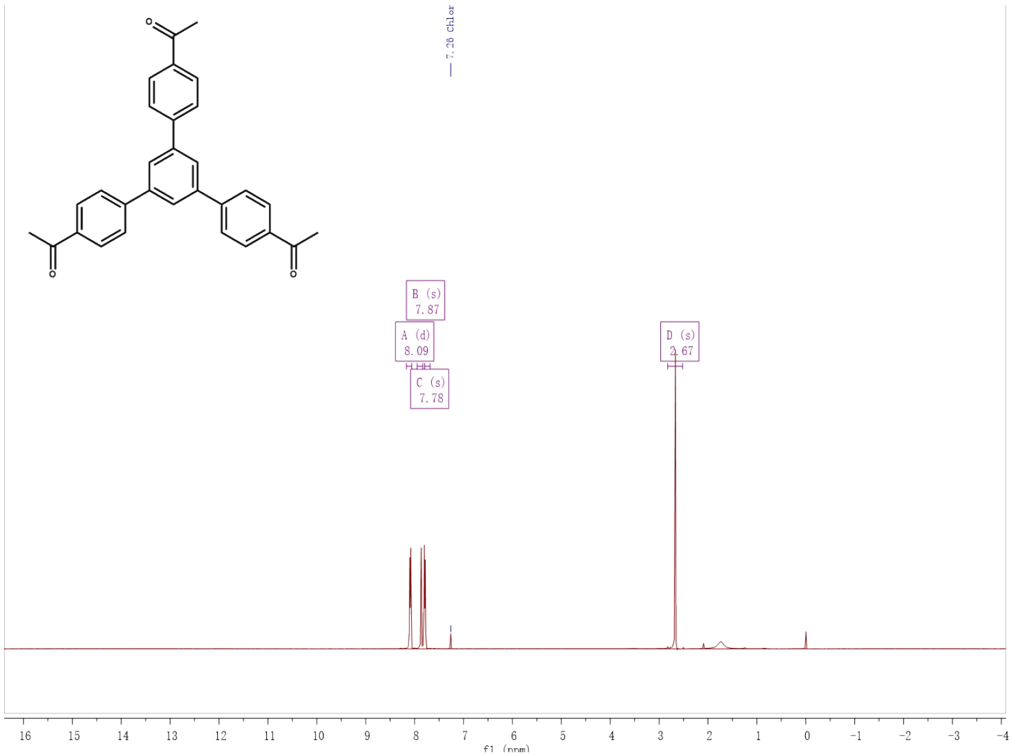

Figure S2. [1]H NMR of 1,3,5-tris(4-acetylphenyl)benzene (TAPB)

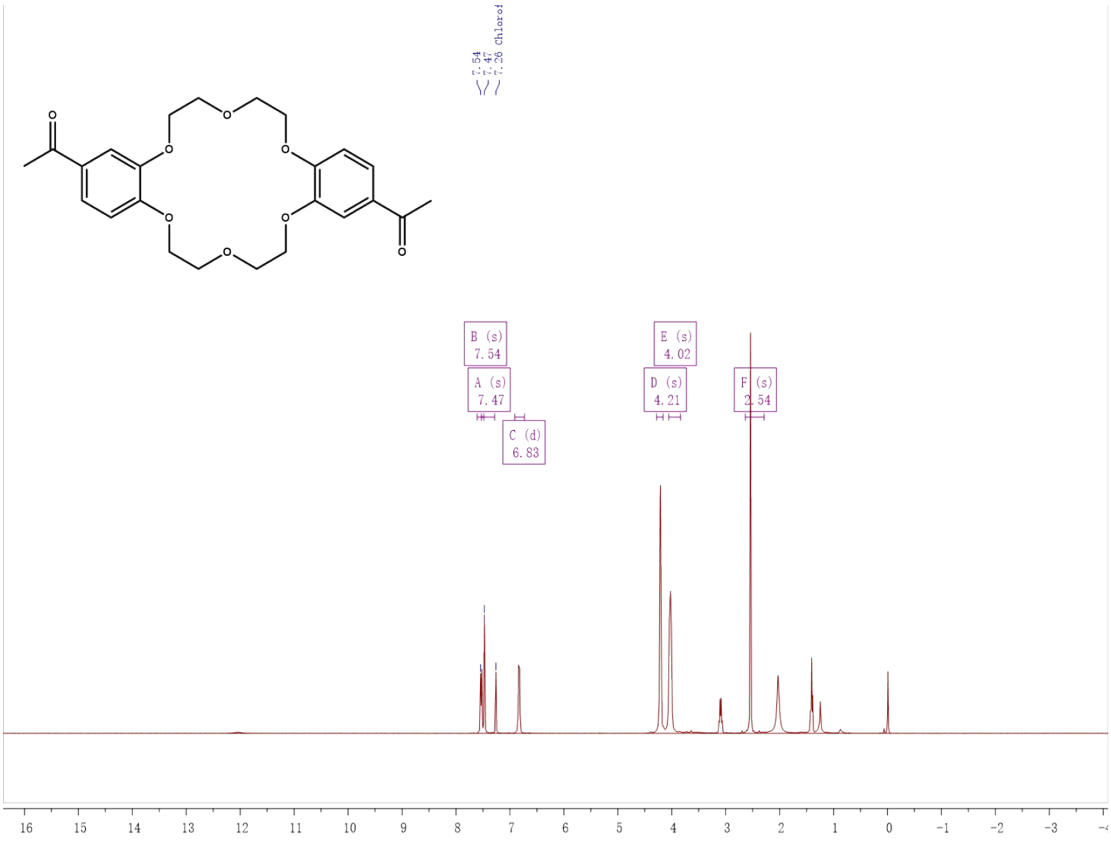

Figure S3. [1]H NMR of 4',4"(5")-Diacetyldibenzo-18-CROWN-6 (DABC)

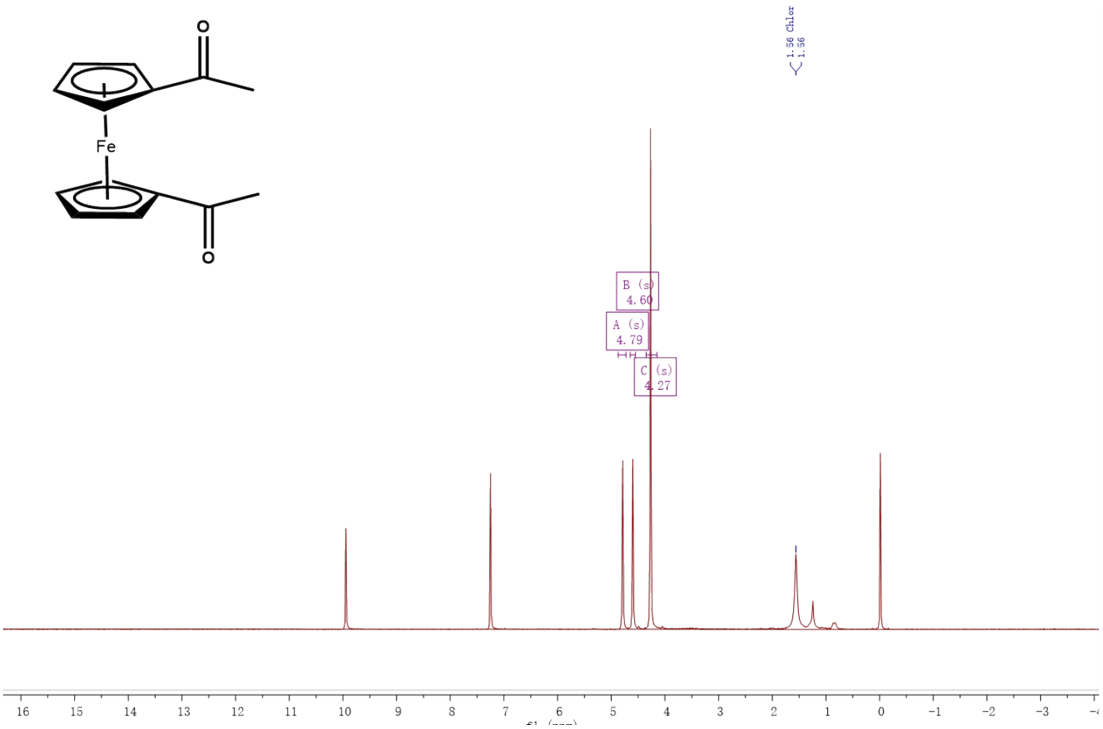

Figure S4. [1]H NMR of 1,1'-Diacetylferrocene (DF)

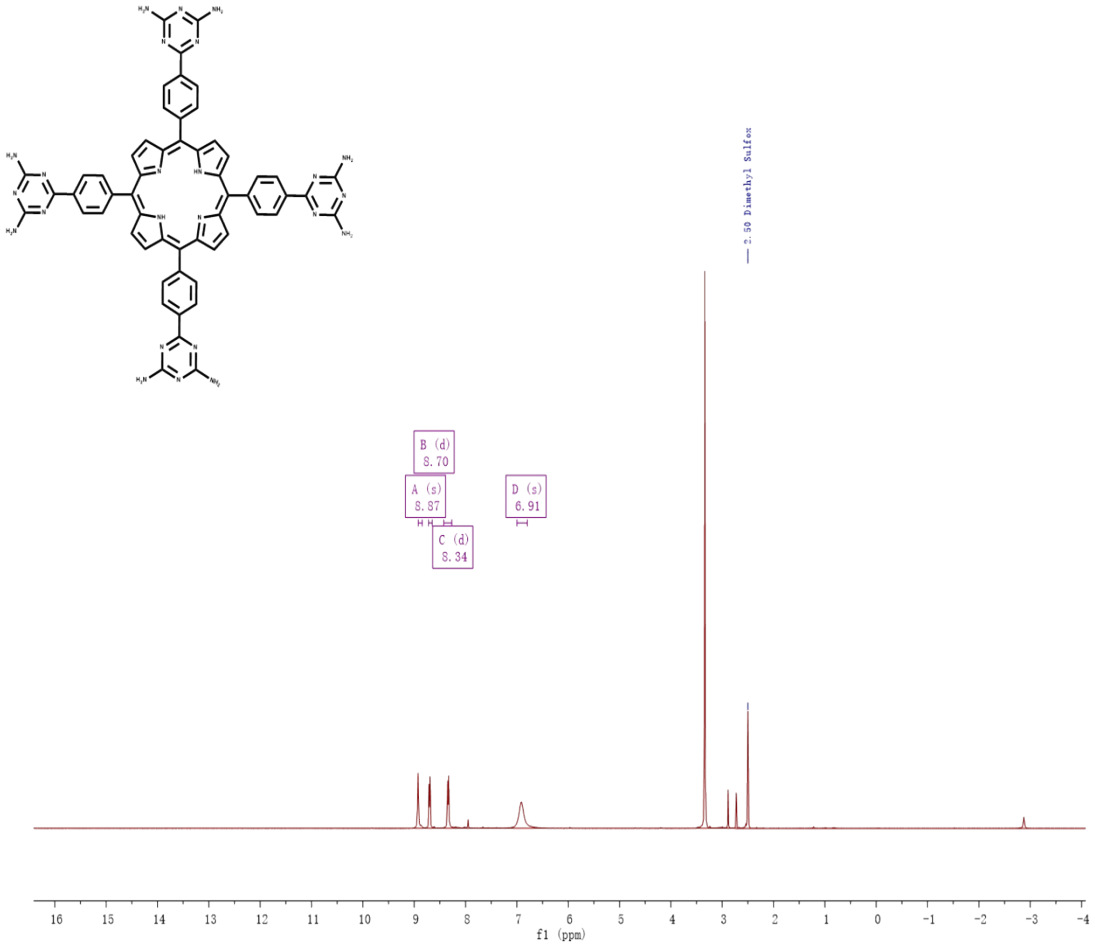

Figure S5. ^{1}H NMR of 5, 10, 15, 20-tetrakis(4-(2,4-diaminotriazine) phenyl) porphyrin (H_2TDPP)

Section 5. FTIR

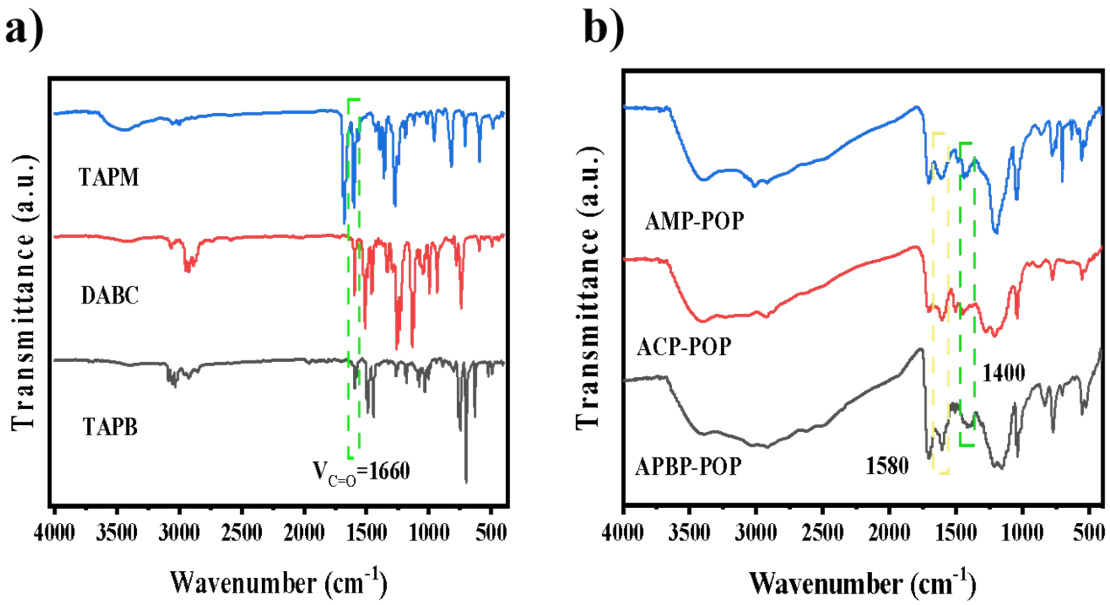

Figure S6. FT-IR Spectroscopy of bridge-engineered POPs.

Section 6. TGA

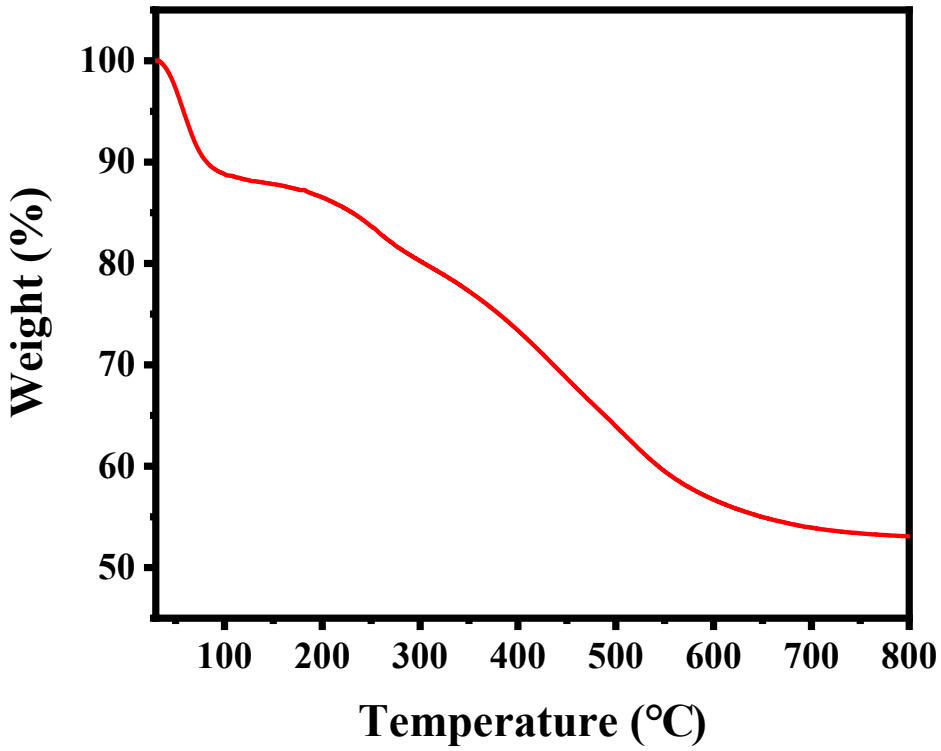

Figure S7. TGA of DFP-POP.

Section 7. EDS and elemental content from TEM mapping

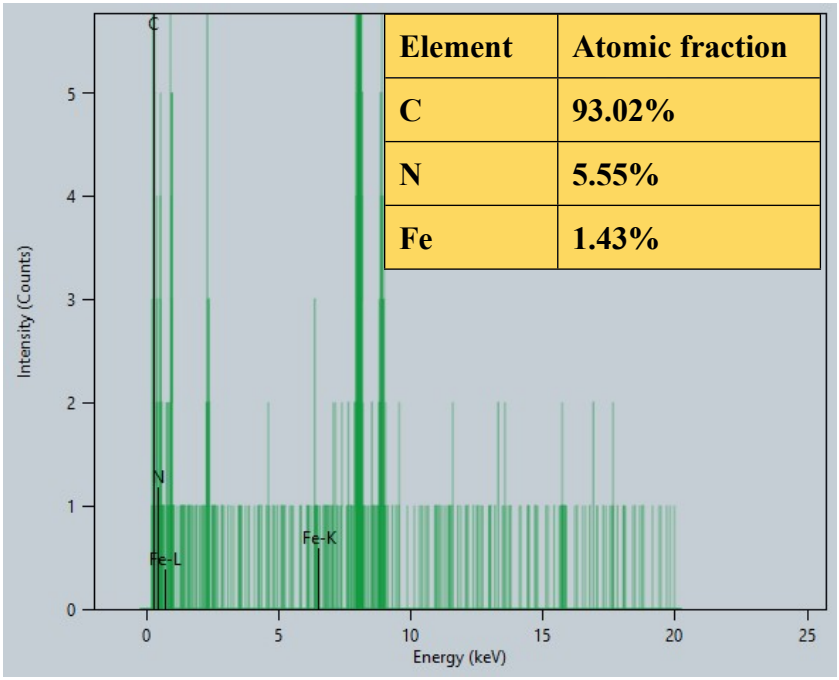

Element	Atomic fraction
C	93.02%
N	5.55%
Fe	1.43%

Figure S8. EDS and elemental content from TEM mapping.

Section 8. The UV-vis-NIR absorption spectroscopy of 1,1'-Diacetylierrocene, H_2TDPP and DFP-POP.

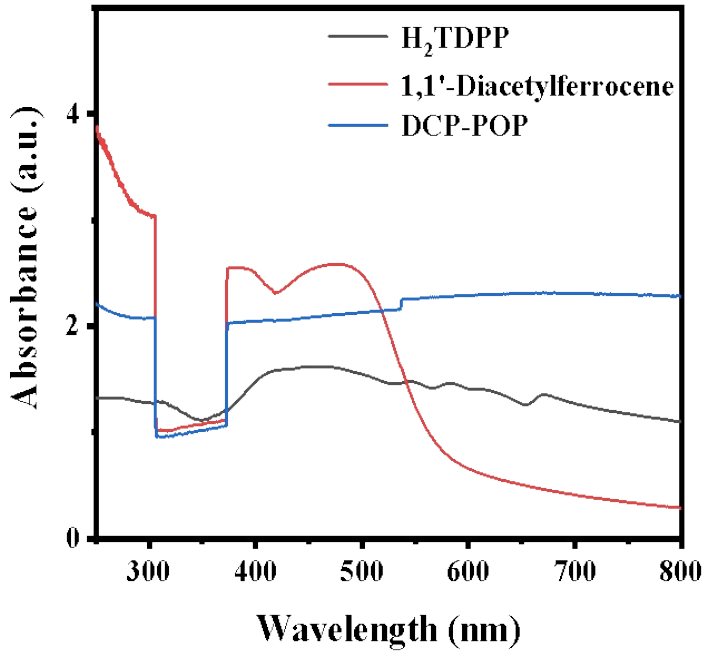

Figure S9. The UV-vis-NIR absorption spectroscopy of 1,1'-Diacetylierrocene (DF),

H_2TDPP and DFP-POP.

Section 9. Photothermograms of AMP-POP, ACP-POP, APBP-POP and DFP-POP

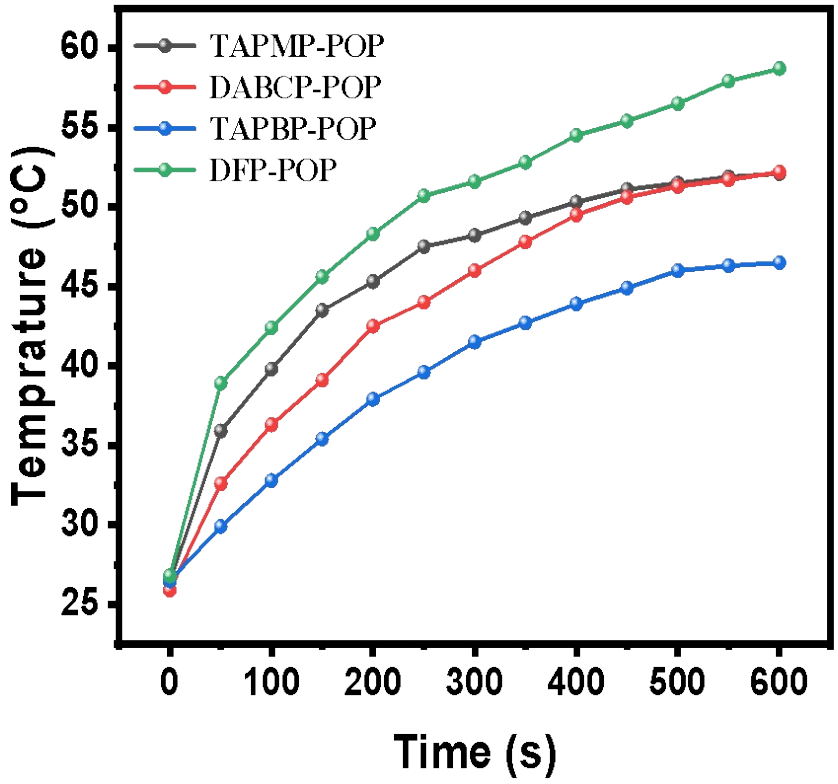

Figure S10. Photothermograms of AMP-POP, ACP-POP, APBP-POP and DFP-POP at 400 μg/mL under laser irradiation (638 nm, 1.0 W/cm², 10 min).

Section 10. Comparison of PCE of different photothermal materials

Table S1.

Samples	**Power Density (W cm^{-2})**	**PCE (%)**	**Reference**
DFP-POP	1.0	43.9	This work
PVA17-g-GO	2.0	39	[7]
AuMC	0.96	25.4	[8]
PDA NPs	1.6	32	[9]
BG-POP	1.0	21.4	[10]
Cu-Fc	1.0	38.4%	[11]
Fe_3O_4-CB@Au-Fc NPs (Au:Fe=1:2)	1.0	36.7%	[12]
Fc-HP°/HD/GOx	1.0	35.6%	[13]
CuS aggregates	1.0	28.43%	[14]
ferrocene-based polymer	2.0	19.25%	[15]
ID@MOS-Fc-CDHA	1.0	18.6%	[16]

Comparison of PCE of recently reported photothermal materials

Section 11. Stability studies of the DFP-POP

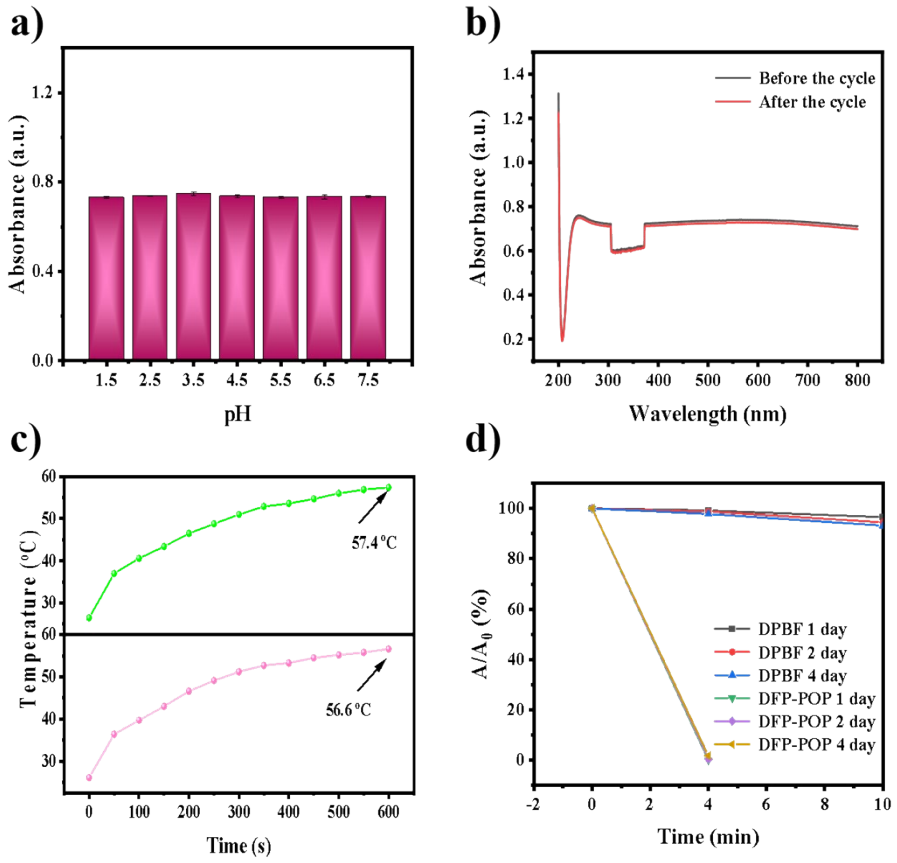

Figure S11. Stability studies of the DFP-POP. a) Stability of DFP-POP in different pH liquids; b) Curves of the DFP-POP before and after the switch cycle; c) Temperature rise curves before and after standing in water for 15 days; d) Decay curves at days 1,2, and 4.

Section 12. UV characteristic peak change of DFP-POP enzyme activity before and after laser irradiation

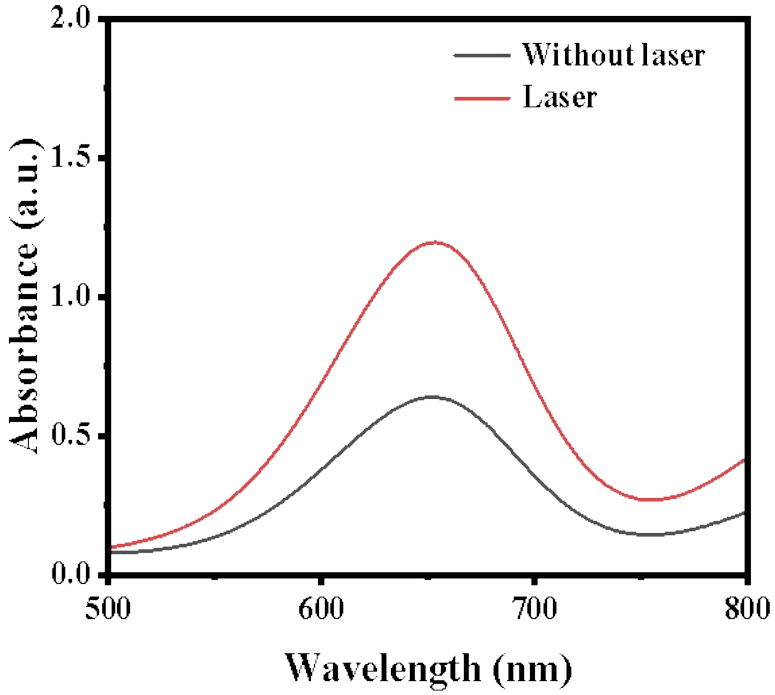

Figure S12. UV characteristic peak change of DFP-POP enzyme activity before and after laser irradiation.

Section 13. UV absorption of different concentrations of H_2O_2

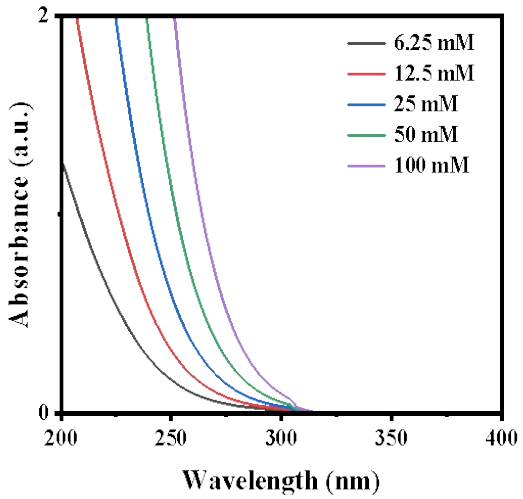

Figure S13. UV absorption of different concentrations of H_2O_2.

Section 14. Synergistic antibacterial graph of DFP-POP at 0-200 μg/mL concentration

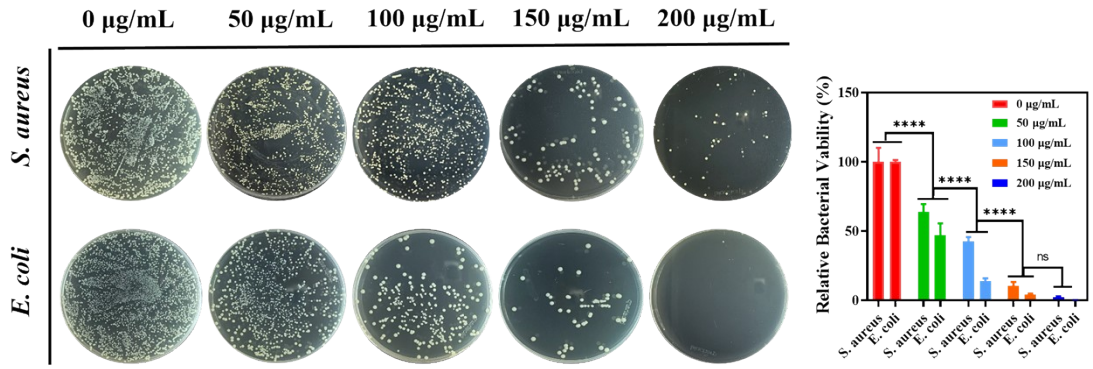

Figure S14. Synergistic antibacterial graph of DFP-POP at 0-200 μg/mL. The H_2O_2 concentration was 10 μL/mL. The laser power density was 1.0 W cm^{-2}. PBS with a solution environment of pH=5.5. Results are presented as mean ± S.D. (* $p < 0.05$, ** $p < 0.01$, *** $p < 0.001$, **** $p < 0.0001$, analyzed by Student's t-test).

Section 15. Comparison of antimicrobial of different materials at 200 μg/mL concentrations

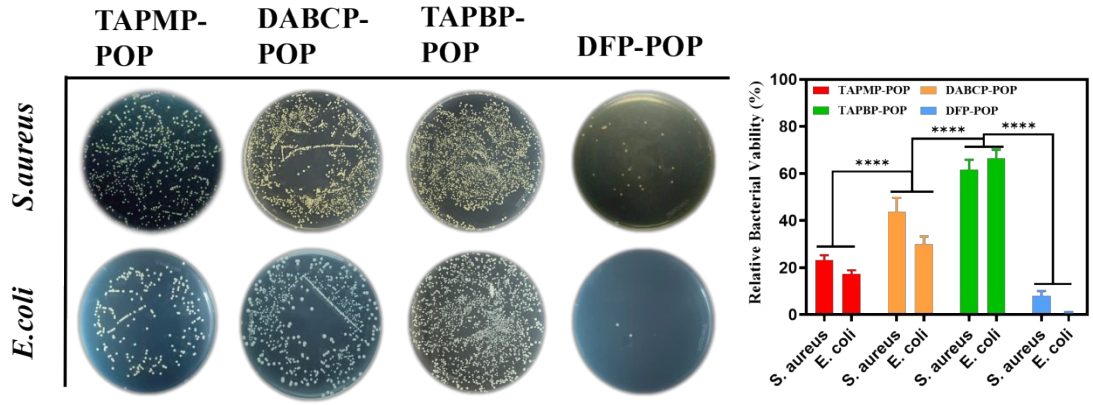

Figure S15. Comparison of antimicrobial of different materials at 200 μg/mL concentrations in the presence of H_2O_2 and Laser illumination. Results are presented as mean ± S.D. (* $p < 0.05$, ** $p < 0.01$, *** $p < 0.001$, **** $p < 0.0001$, analyzed by Student's t-test).

Section 16. Performance comparison of recently reported polymer-based antibacterial agents

Table S2. Performance comparison of recently reported polymer-based antibacterial agents

Sample	**Antibacterial mode**	***E. coli***	***S. aureus***	**Reference**
DFP-POP (200 μg/mL)	PTT (638 nm, 1.0W/cm^2, 10min)/PDT/CAT/POD	99.52%	96.81%	This work
Pre-NP-4 (333 μg/mL)	NO/PTT (808 nm, 375 mW/cm^2, 5min)	100%	100%	[17]
IM-POP-Ag (200μg/mL)	Ag ions/imidazole	>96.4%	>93.7%	[18]
AFcB (500 μg/mL)	1,2,3-triazole, Ferrocene, xanthone, and azine units	99.9%	99.9%	[19]
PdPPOP HBTT (200 μg/mL)	PDT/PTT (808nm, 0.7W/cm^2, 20min)	96.9%	100%	[20]
FePPOP BFPB (500 μg/mL)	PDT (808 nm, 1.2W/cm^2, 20 min)	--	90%	[21]

Section 17. Thermography maps of the mouse back wounds at varied time points

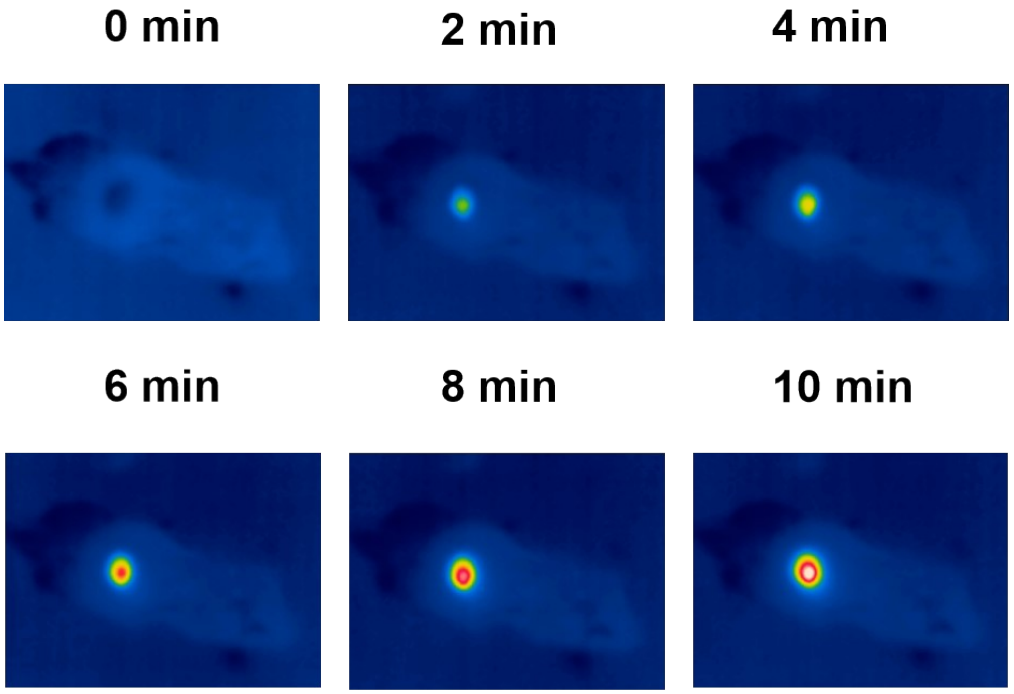

Figure S16. Thermography maps of the mouse back wounds.

Section 18. H&E and Masson trichrome stained wound tissue sections of mice on day 9

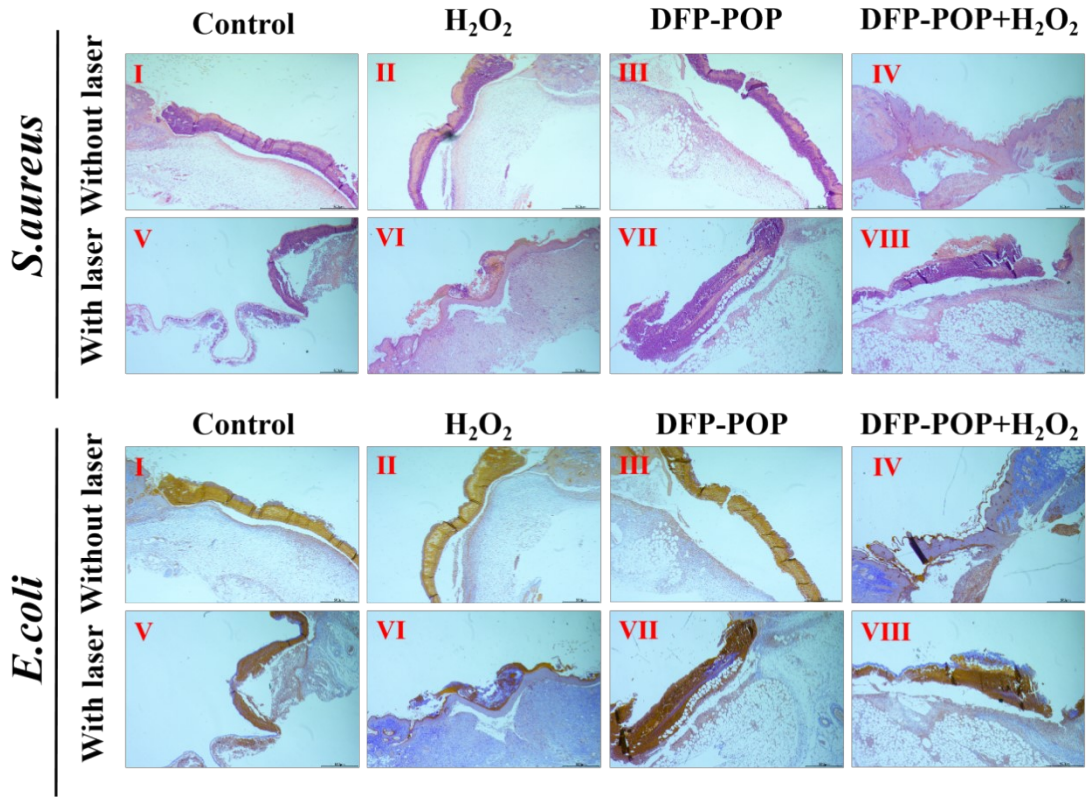

Figure S17. H&E and Masson trichrome stained wound tissue sections of mice on day 9

Section 19. Supporting References

[1] Yang, Z., Chen, H., Li, B., Guo, W., Jie, K., Sun, Y., Jiang, D.E., Popovs I., Dai, S. Topotactic Synthesis of Phosphabenzene-Functionalized Porous Organic Polymers: Efficient Ligands in CO_2 Conversion. Angew. Chem. Int. Ed., 2019, 58, 13763-13767.

[2] Luk'yanenko, N. G., Bogat-skii, A. V., Pastushok, V. N., Kulygina, Yu. E., Berdnikova L. R., Mamina, M. U. Macroheterocycles. 7. Synthesis and extraction capacity of some dibenzo-18-crown-6-derivatives. Chem Heterocycl Compd. 1981, 17, 433–437.

[3] Cui, Y., Zhao, Y., Wang, T., Han. B., Benzimidazole−Linked Porous Polymers: Synthesis and Gas Sorption Properties. Chinese J. Chem. 2015, 33, 131-136.

[4] Fomin V. M., Shuklina N. N. Effect of the Nature of the Solvent on the Formation of Ferrocene Cations during the Protonation of Acetil- and 1,1'-Diacetylferrocene with Perchloric Acid and Their Oxidation with Iodine. Russian J. Phys. Chem. A 2023, 97, 1376-1381.

[5] Dahal, S., Goldberg, I. Solid−state supramolecular chemistry of porphyrins. Hydrogen-bonded networks and porous crystals of meso-tetra [4-(3,5-diaminotriazino) phenyl] porphyrin. J. Phys. Organic Chem. 2000, 13, 382-387.

[6] He, J., Wang, Y., Yuan, J., Liu, C., Pan, C., Weng, Z., Tang, X., Liu, Y., Yu. G. Ferrocene-integrated conjugated microporous polymer nanosheets: Active and regenerative catalysts for photomediated controlled radical polymerization. Applied Materials Today, 2020, 18, 100507-100507.

[7] Yu, J., Zhang, J., Han, W., Liu, B., Guo, W., Li, L., Li, N., Wang, Z., Zhao, J. Enhanced cryopreservation performance of PVA grafted monolayer graphite oxide with synergistic antifreezing effect and rapid rewarming. Composites Science and Technology, 2024, 247, 110404.

[8] Zhang, W., Cai, K., Sun, Z., Xiang, Q., Yuan, L., Fu, M., Liu, X., Foda, Mohamed F. F., Ye, Z., Huang, J., Liu, H., Han, H., Liang, H., Dong, H., Zhang, X. Elevating Second Near-Infrared Photothermal Conversion Efficiency of Hollow Gold

Nanorod for a Precise Theranostic of Orthotopic Bladder Cancer. ACS Nano, 2023, 17, 18932-18941.

[9] Zhang, Y., Zhang, K., Yang, H., Hao, Y., Zhang, J., Zhao, W., Zhang, S., Ma, S., Mao, C. Highly Penetrable Drug-Loaded Nanomotors for Photothermal-Enhanced Ferroptosis Treatment of Tumor. ACS. Appl. Mater. Interfaces., 2023, 15, 14099.

[10] Wang, J., Zhang, X., Wang, N., Wang, J., Kong, H., Li, J., Zhang, G., Du, H., Zhou, B., Wang, B. Nanoporous BODIPY-Based Cationic Porous Organic Polymer Composites as Photocontrolled NO-Releasing Platforms for Wound Healing and Antimicrobial Applications. ACS Appl. Nano Mater. 2023, 6, 16716-16729.

[11] Yang, J., Yang, L., Li, Q., Zhang, L. Ferrocene-based multifunctional nanoparticles for combined chemo/chemodynamic/photothermal therapy. J. Colloid Interface Sci. 2022, 626, 719-728.

[12] Cheng, Q., Yue, L., Li, J., Gao, C., Ding, Y., Sun, C., Xu, M., Yuan, Z., Wang, R. Supramolecular Tropism Driven Aggregation of Nanoparticles In Situ for Tumor-Specific Bioimaging and Photothermal Therapy. Small, 2021, 17, e2101332-e2101332.

[13] Lee, S. Y., Park, J., Jeong, D. I., Hwang, C., Lee, J., Lee, K., Kim, H., Cho, H. J. Ferrocene and glucose oxidase-installed multifunctional hydrogel reactors for local cancer therapy. J. Controlled release, 2022, 349617-633.

[14] Li, J., Cheng, Q., Yue, L., Gao, C., Wei, J., Ding, Y., Wang, Y., Zheng, Y., Wang, R. Macrophage-hitchhiking supramolecular aggregates of CuS nanoparticles for enhanced tumor deposition and photothermal therapy. Nanoscale Horizons, 2021, 6, 907-912.

[15] Zhu, W., Zhang, C., Chen, Y., Deng, Q. Synthesis of Magnetic Ferrocene-Containing Polymer with Photothermal Effects for Rapid Degradation of Methylene Blue. Polymers, 2021,13, 558-558.

[16] Choi, H. W., Lim, J. H., Kang, T., Chung, B. G. Antioxidant, Enzyme, and H_2O_2-Triggered Melanoma Targeted Mesoporous Organo-Silica Nanocomposites for Synergistic Cancer Therapy. Antioxidants. Antioxidant, Enzyme, and H_2O_2-Triggered Melanoma Targeted Mesoporous Organo-Silica Nanocomposites for Synergistic

Cancer Therapy. Antioxidants, 2022, 11, 2137-2137.

[17] Bao, X., Zheng, S., Zhang, L., Shen, A., Zhang, G., Liu, S., Hu, J. Nitric-Oxide-Releasing aza-BODIPY: A New Near-Infrared J−Aggregate with Multiple Antibacterial Modalities. Angew. Chem. Int. Ed. 2022, 134, e202207250.

[18] Luo, H., Huang, T., Li, X., Wang, J., Lv, T., Tan, W., Gao, F., Zhang, J., Zhou B. Synergistic antibacterial and wound-healing applications of an imidazole-based porous organic polymer encapsulated silver nanoparticles composite. Microporous Mesoporous Mater. 2022, 337, 111925.

[19] Lakouraj, M. M., Hasantabar, V., Tashakkorian, H., Golpour, M. Novel anticancer and antibacterial organometallic polymer based on ferrocene as a building block and xanthone bioactive scaffolds: Synthesis, characterization, and biological study. Polymers for Advanced Technologies, 2018, 29, 2784-2796.

[20] Li, Y., Wang, Q., Qu, X., Tian, J., Zhang, X. Construction of palladium porphyrins and triptycene photo-activated nanomaterial for enhanced colorimetric detection and inactivation of bacteria. J. Colloid Interface Sci. 2023, 648 220-230.

[21] Li, D., Fang, Y., Zhang, X. Bacterial Detection and Elimination Using a Dual-Functional Porphyrin-Based Porous Organic Polymer with Peroxidase-Like and High Near-Infrared-Light-Enhanced Antibacterial Activity. ACS Appl. Mater. Interfaces 2020, 12, 8989-8999.